First-principles calculations of phonon and thermodynamic properties in the boron-alkaline earth metal binary systems: B-Ca, B-Sr, and B-Ba

Shunli Shang,* Yi Wang, and Zi-Kui Liu
Department of Materials Science and Engineering, The Pennsylvania State University, 304 Steidle Building, University Park, Pennsylvania 16802, USA

(Received 24 July 2006; revised manuscript received 30 October 2006; published 16 January 2007)

The phonon and thermodynamic properties of the divalent alkaline-earth hexaborides, MB_6 (M=Ca, Sr, Ba), and the reference elements α-B, fcc-Ca, fcc-Sr, and bcc-Ba are investigated on the basis of first-principles projector augmented wave method together with the quasiharmonic phonon calculations. The calculated phonon dispersion relations by using the supercell approach are in good agreements with those obtained by the inelastic neutron scattering, Raman scattering, and infrared absorption. The experimentally revealed anomalous behaviors of phonon dispersions in the alkaline-earth metals are correctly predicted; i.e., for both fcc-Ca and fcc-Sr, the frequency of the lower transverse $[\xi\ \xi\ 0]$ branch exhibits slightly positive dispersion, and for bcc-Ba the frequency of the longitudinal branch along the $[\xi\ 0\ 0]$ direction is lower than that of the transverse branch. These anomalous phenomena can be traced back to the effect of d electron. The predicted phonon dispersion relations among CaB_6, SrB_6, and BaB_6 show similar features except that the frequencies decrease from CaB_6, SrB_6, to BaB_6 due to the influence of mass. It is also found that the low frequency T_{1u} modes of CaB_6, SrB_6, and BaB_6 have large LO/TO splitting (greater than 5 THz). To that end, the finite temperature thermodynamic properties (entropy, enthalpy, and Gibbs energy) of MB_6 (M=Ca, Sr, Ba) and elements B, Ca, Sr, and Ba are calculated; herein, both the electronic and phonon contributions are considered. This work indicates that the difference of the enthalpies of formation of CaB_6, SrB_6, and BaB_6 is small (less than 4 kJ/mol instead of the measured 30 kJ/mol), which agrees with the facts that they possess the similar phonon dispersion relations, melting temperatures, bulk moduli, and Debye temperatures.

DOI: 10.1103/PhysRevB.75.024302 PACS number(s): 63.20.Dj, 65.40.Gr, 75.50.−y, 71.20.−b

I. INTRODUCTION

The divalent alkaline-earth hexaborides, MB_6 (M=Ca, Sr, Ba), are usually known for having properties of low density, low coefficient of thermal expansion, high melting point, high hardness, and good chemical stability.[1,2] Recently, the discovery of anomalous ferromagnetism in La-doped CaB_6, SrB_6, and BaB_6 (Ref. 3) has attracted great interests because of (i) the low magnetic moment ($\leqslant 0.07\mu_B$ per La atom for CaB_6), (ii) the very high Curie temperature (>600 K for CaB_6), and (iii) the absence of elements with partially filled d or f orbitals which are usually required for ferromagnetism. Considerable experimental and theoretical work towards understanding this unexpected phenomenon is carried out, especially for CaB_6.[4–11] Currently it seems conclusive that the ferromagnetism of CaB_6 (also should be true for SrB_6 and BaB_6 due to their similar structures) is caused by the external impurities on the surface of the sample rather than an intrinsic property, and CaB_6 is not an intrinsic semimetal but a semiconductor with band gap greater than 1 eV at the X point of the simple cubic Brillouin zone.[7,9] Instead of exploring again the origin of ferromagnetism and the band structures of the divalent alkaline-earth hexaborides, it is interesting to study the phonon properties in these compounds since few investigations are performed, in particular for SrB_6 and BaB_6 (see Sec. IV C). On the other hand, the lattice dynamics can serve as a starting point to study the finite temperature thermodynamics, which is far from fully understood; e.g., the large difference among the measured enthalpies of formation for CaB_6, SrB_6, and BaB_6 (−17, −30, and −47 kJ/mol,[12] respectively) is doubtful due to the similar properties are expected among them.

The present work aims at providing a fundamental investigation on the phonon and thermodynamic properties of CaB_6, SrB_6, and BaB_6 together with the reference elements α-B, fcc-Ca, fcc-Sr, and bcc-Ba starting from the first-principles calculations within the density functional theory. To our knowledge, the present available first-principles calculations still suffer from an inadequate description of both the structure properties and the semiconductor natures for the alkaline-earth hexaborides (e.g., CaB_6). The pseudopotential GW (G being the Green function and W the screened Coulomb interaction) calculation predicts a 0.8 eV band gap at the X point for CaB_6 (Ref. 4). However, other GW calculations based on the linear-muffin-tin-orbital (LMTO) method show widely different band gap values, or no such gap.[9,13] In addition, the calculation of exact total energy by using the GW method is still in developing,[14] which is more interesting to the present investigation. The weighted density approximation (WDA) (Ref. 8) and the screened-exchange local density approximation (sX-LDA) (Ref. 9) also could predict the correct band gap (0.8 eV by WDA and >1.2 by sX-LDA). While the predicted structure parameters are less accurate, the predicted internal positional parameter x of the B atom (see Sec. IV C for details) is 0.206 by WDA and 0.212 by sX-LDA (the recently measured value is 0.202,[15] see Sec. IV C). Additionally the predicted phonon frequency of breathing mode by sX-LDA is also inaccurate (see Sec. IV C). It might be because the structure properties are not predicted accurately. Since the highly accurate prediction of structure properties can be achieved by using the local density approximation (LDA) or the generalized gradient approximation (GGA), which is a prerequisite to perform the

accurate phonon calculation. The GGA is therefore employed in this work, although it can only predict a semimetallic band structure for the alkaline-earth hexaborides;[16] the phonon properties are correctly calculated as demonstrated in this work.

The first-principles phonon calculations are essentially performed by the linear response method and the supercell method.[17] The supercell method, in which the forces are calculated with respect to the atoms displaced from their equilibrium positions and frozen in, can be easily applied to quite complex crystal structure, and thus adopt in the present research (see detailed interpretation in Sec. II). The finite temperature thermodynamic properties are calculated from the obtained phonon density of states (DOS's). The anharmonic contributions are taken into account by the quasiharmonic approximation. As indicated by Wang *et al.*,[18] the electron also has considerable contributions at high temperatures to the thermodynamic properties, in particular for the cases with more electronic DOS's at the Fermi level; thus, the electron contributions are also included.

This paper is organized as follows. In Sec. II, the theories of the phonon calculation and the calculations of thermodynamic properties from the electronic DOS's and phonon DOS's are outlined. In Sec. III, the methodology to perform the first-principles phonon calculations is presented. In Sec. IV, we discuss the obtained properties of B, Ca, Sr, Ba, CaB_6, SrB_6, and BaB_6, including (i) the equilibrium structure properties, (ii) the electronic DOS's, (iii) the phonon dispersion relations and the pressure vs phonon frequency relations at high symmetry points, and (iv) the thermodynamic properties (entropy, enthalpy, and Gibbs energy) including both phonon and electronic contributions. Finally, in Sec. V the conclusions of the present work are given.

II. THEORY

The physics of phonon is typically described by the harmonic approximation, in which the equation of motion is written as[19]

$$\omega^2(\boldsymbol{k},l)\boldsymbol{e}(\boldsymbol{k},l) = \boldsymbol{D}(\boldsymbol{k})\boldsymbol{e}(\boldsymbol{k},l). \tag{1}$$

The solution of this eigenvalue function gives the eigen (phonon) frequencies $\omega(\boldsymbol{k},l)$ with respect to wave vector $\boldsymbol{k}$ and phonon mode l, and the eigen (polarization) vectors $e(\boldsymbol{k},l)$ describing the corresponding atomic displacements. $\boldsymbol{D}(\boldsymbol{k})$ is the dynamic matrix, which can be obtained from the force constant matrix $\boldsymbol{\Phi}$

$$\boldsymbol{D}_{st}^{\alpha\beta}(\boldsymbol{k}) = \frac{1}{\sqrt{M_s M_t}} \sum_{\boldsymbol{R}} \boldsymbol{\Phi}_{st}^{\alpha\beta}(\boldsymbol{R}) \exp(-\mathrm{i}\boldsymbol{k}\cdot\boldsymbol{R}), \tag{2}$$

where M_s and M_t are masses for atoms s and t, respectively, $\boldsymbol{R}$ the Bravais lattice vectors, α, β=x, y, and z in three dimension. Within the framework of harmonic approximation, keeping only the second terms in the Taylor series of total energy E, $\boldsymbol{\Phi}$ is given by

$$\boldsymbol{\Phi}_{st}^{\alpha\beta} = \frac{\partial^2 E}{\partial u_s^{\alpha} \partial u_t^{\beta}}, \tag{3}$$

where u_s^{α} is the displacement of atom s from its equilibrium position in α direction. Consequently the force $\boldsymbol{f}$ exerted on atom s relating the displacement of atom t is,

$$\boldsymbol{f}_s = -\boldsymbol{\Phi}_{st} u_t. \tag{4}$$

The starting point to solve Eq. (1) is to determine the dynamical matrix, which is essentially performed by the linear response method (LRM) and the supercell method (also known as frozen phonon method[17] or direct approach[20]) in terms of first-principles phonon calculations.[17] The LRM determines directly the dynamic matrix for a set of k points in the Brillouin zone. The LRM is exact due to taking into account arbitrarily long-range force, while the limit of LMR arises from the use of small number of k points. The supercell method[17] determines the dynamical matrix starting from Eq. (4), in which the forces are calculated with respect to the atoms perturbed from their equilibrium positions and frozen in. The supercell method is less accurate in comparison with LRM since a finite range of forces is considered. However, the supercell method has the advantages of (i) faster computing by appropriate choices of supercell and perturbations and (ii) easier implementation, and therefore can be easily applied to quite complex crystal structures.[21] In the case of the studied properties, e.g., thermodynamic properties in this work, which are less sensitive to the accuracy of phonon calculation, the supercell method should be a good choice and thus are adopted here.

From the ω vs $\mathbf{k}$ dispersion relations solved through Eq. (1), the distribution of ω, i.e., the phonon DOS's $g(\omega)$, can be determined, and in consequence the free energy per primitive unit cell can be written down according to the partition function of lattice vibration

$$F_{ph}(T) = k_{\mathrm{B}}T \int_0^{\infty} \ln\left[2 \sinh \frac{\hbar\omega}{2k_{\mathrm{B}}T}\right] g(\omega) d\omega, \tag{5}$$

where T is the temperature, k_B the Boltzmann constant, and $\hbar$ the Planck constant. Consequently from the electronic DOS's, the electronic free energy (F_{el}=E_{el}−TS_{el}) can be determined. The electronic energy due to the electronic excitations is given by[18]

$$E_{el}(T) = \int n(\varepsilon) f \varepsilon d\varepsilon - \int^{\varepsilon_F} n(\varepsilon)\varepsilon d\varepsilon, \tag{6}$$

where $n(\varepsilon)$ are the electronic DOS's, ε the energy eigenvalues, f the Fermi distribution function, and ε_{F} the energy at the Fermi level. The total electronic numbers below the Fermi level at 0 K are assumed to be constant during the estimation of ε_{F} at the temperature of interest. The electronic entropy in the mean field approximation is written by[18,22]

$$S_{el}(T) = -k_{\mathrm{B}} \int n(\varepsilon)[f \ln f + (1-f)\ln(1-f)] d\varepsilon. \tag{7}$$

Within the quasiharmonic approximation, the anharmonic effect can be accounted by the harmonic approximation at several different volumes. In this case, the free energy can be approximated as

TABLE I. Details to perform the first-principles and phonon calculations, including the Pearson's symbol and the space group of pure element or compound, the valence states of pure element used in the PAW potential, the cutoff energy (E_{cut} in eV) for plane wave basis, k mesh used to calculate the electronic and phonon structures, the amount of atoms in the supercell (SC atoms) to perform the phonon calculation, the displacement (Δr in Å) of disturbed atom from its equilibrium position, and the cutoff distance (R_{cut} in Å) used to specify the fitting range of force constants.

Material	Pearson symbol	Space group	Valence states	E_{cut} (eV)	k-mesh electron	SC atoms	k-mesh phonon	Δr (Å)	R_{cut} phonon (Å)
fcc-Ca	$cF4$	$Fm\bar{3}m$	$3s^2 3p^6 4s^2$	370	$22\times22\times22$	32	$6\times6\times6$	0.2	7.0
fcc-Sr	$cF4$	$Fm\bar{3}m$	$4s^2 4p^6 5s^2$	290	$22\times22\times22$	32	$6\times6\times6$	0.2	8.0
bcc-Ba	$cI2$	Im $\bar{3}m$	$5s^2 5p^6 6s^2$	240	$22\times22\times22$	32	$6\times6\times6$	0.4	7.5
CaB_6	$cP7$	$Pm\bar{3}m$		420	$18\times18\times18$	56	$6\times6\times6$	0.06[a]	6.0
SrB_6	$cP7$	$Pm\bar{3}m$		420	$18\times18\times18$	56	$6\times6\times6$	0.05	6.5
BaB_6	$cP7$	$Pm\bar{3}m$		420	$18\times18\times18$	56	$6\times6\times6$	0.06	6.5

[a]Larger displacement 0.1 Å is adopted for lattice parameters larger than $1.01\times a_0$.

$$F(V,T) = E_0(V) + F_{ph}(V,T) + F_{el}(V,T), \tag{8}$$

where $E_0(V)$ is the first-principles ground state energy at 0 K and volume V, $F_{ph}(V,T)$ is the phonon contributions to free energy given by Eq. (5) at each V, and $F_{el}(V,T)$ the electronic contributions given by Eqs. (6) and (7) with respect to the corresponding V and T. The equilibrium free energy F at each temperature T can be obtained by minimizing Eq. (8) with respect to V. In the present work, the F vs V curves are fitted to a four-parameter equation of state for the temperatures of interest; consequently, the equilibrium free energy, volume, bulk modulus, and the pressure derivative of the bulk modulus can be estimated, see Ref. 23 for details.

III. METHODOLOGY

In the present work, the first-principles calculations are performed by using the projector-augmented wave (PAW) method[24] as implemented in VASP.[25] The generalized gradient approximation (GGA) (Ref. 26) is used for the exchange-correlation potential. The PAW potential is adopted to describe the electron-ion interaction because of its efficient implementation of force, and meanwhile it combines the accuracy of all-electron methods with the efficiency of pseudopotentials. The phonon calculations are carried out by the supercell method[17] as implemented in ATAT code.[27] More details of the first-principles phonon calculations for each structure are shown in Table I, including (i) the Pearson's symbol and the space group; (ii) the treatment of valence states in the PAW potential; (iii) the energy cutoff on the wave functions, which is about 1.25 to 1.3 times higher than the default one; (iv) the size of k mesh for electronic structure calculations, which is constructed using the Monkhorst-Pack scheme;[28] (v) the setting of supercell (denoted by the amount of atoms per supercell) used to perform the phonon calculations; (vi) the size of k mesh for the calculations of force acting on atoms in the perturbed supercell; (vii) the setting of displacement from the equilibrium atomic positions, giving a maximum force around 0.5 eV/Å (0.3~0.9); and (viii) the setting of cutoff range used to fit the force constants. Convergences of properties, such as total energy and phonon dispersion, have been checked for the aforementioned settings in Table I. All the structures shown in Table I are fully relaxed and the final static calculations (to obtain electronic DOS's and accurate total energies) using tetrahedron smearing method with Blöchl corrections[29] are employed in the present work.

IV. RESULTS AND DISCUSSIONS

In this section, the calculated equilibrium lattice parameters (or volumes for α- and β-B), bulk moduli (both at 0 K and room temperature), electronic DOS's, and phonon dispersion relations, together with the predicted finite temperature thermodynamic properties (entropy, enthalpy, and Gibbs energy), are presented and compared with the available experimental data for α- and β-B (Sec. IV A), alkaline-earth metals Ca, Sr, and Ba (Sec. IV B), and alkaline-earth hexaborides CaB_6, SrB_6, and BaB_6 (Sec. IV C).

A. α- and β-boron

Boron (B) is one of the fascinating elements due to its superconductivity at high pressure,[30] semiconductivity, and the vast variety of polymorphs,[31] of which a B_{12} icosahedron is the basic structure unit. α-B ($hR12$) is the simplest one consisting of one distorted icosahedron in a rhombohedral structure. β-B ($hR105$ for the ideal configuration) is the most commonly found modification in a complex rhombohedral structure. The phase stability in α- and β-B has been studied in terms of first-principles quasiharmonic phonon calculations by the present authors.[32] Table II summarizes the calculated properties of α- and β-B at 0 K (without the phonon contribution) and 298 K (with the phonon contribution), including the lattice parameters, volume, bulk modulus, pressure derivative of bulk modulus, thermal expansion coefficient, and the second-moment Debye temperature.[33] The predicted properties, especially the results at room temperature (298 K), are in good agreements with the experimental

TABLE II. Calculated properties of α- and β-B at 0 K (without phonon contribution) and 298 K (with phonon contribution) together with the experimental data, including the lattice parameters a_0 and c_0 (Å) in hexagonal setting, volume V_0 (Å^3/atom), bulk modulus B_0 (GPa), pressure derivative of bulk modulus B_0' thermal expansion coefficient γ (10^{-6} K^{-1}), and the Debye temperature Θ_D (K).

Material		a_0 (Å)	c_0 (Å)	V_0 Å^3/atom	B_0 (GPa)	B_0'	γ (10^{-6} K^{-1})	Θ_D (K)
α-B	0 K	4.902	12.545	7.253	209.10	4.08		1372[a]
	298 K	4.926[b]	12.605[b]	7.360	201.70	3.97	3.74	
	Experiment	4.924[c]	12.610[c]	7.355[c]	213(15)[d]	3.5[e]		1430[f]
β-B	0 K	10.919	23.724	7.776	193.42	4.33		1288[a]
	298 K	10.972[b]	23.839[b]	7.890	181.17	4.42	4.52	
	Experiment	10.925[g]	23.814[g]	7.822[g]	185(7)[d]	4.0[d]	6.4[h]	1300[f]

[a]Estimated from the second-moment Debye cutoff frequency obtained by phonon DOS.
[b]Estimated from the volume at 298 K assuming the same c/a ratio as 0 K.
[c]X-ray diffraction (XRD) (Ref. 34).
[d]XRD of α-B and neutron diffraction of β-B (Ref. 35).
[e]LDA calculation (Ref. 36).
[f]Reference 37.
[g]Reference 38.
[h]Average value in the temperature range 293–1023 K (Ref. 39).

data.[34–39] The larger volume, and the lower bulk modulus and Debye temperature of β-B with respect to those of α-B, indicate the weakening of covalent bonds in β-B. The predicted pressure derivative of bulk modulus of β-B is larger than that of α-B, consistent with the larger thermal expansion coefficient of β-B, implying the further weakening of covalent bonds of β-B at elevated temperatures. It is also worth mentioning that the predicted Wyckoff sites in β-B are in excellent agreements with the measurements[38,40] with the average standard deviations of 0.0013. The first-principles phonon calculations in Ref. 32 indicate that (i) α-B is more stable than β-B at lower temperatures up to the predicted 1388 K, and the thermodynamic stability of β-B at high temperatures ascribes to the higher phonon DOS at the lower frequency region with respect to that of α-B; (ii) the defect-free β-B is unstable at high temperatures (above 1840 K) indicated by the appearance of imaginary phonon modes. Extra B atoms are needed at high temperatures in order to prevent the formation of imaginary phonon modes of the defect-free β-B. The predicted thermodynamic properties in Ref. 32 by considering only phonon contribution will be adopted here. The electronic contributions are neglected due to the semiconductor natures of α- and β-B (see also Sec. IV C). In the present work, the α-B is set as reference state of element B due to its stability at low temperatures.

B. Ca, Sr, and Ba

The divalent alkaline-earth metals Ca, Sr, and Ba possess a number of interesting properties. For instance, their crystal structures exhibit as a function of temperature and pressure.[41,42] At ambient condition, the stable structure is fcc for Ca and Sr, and bcc for Ba.[42] Ca and Sr are known as semimetal; at lower pressure, Ca and Sr display a metal-nonmetal transition in which the metallic character is lost.[43] The divalent alkaline-earth metals (e.g., Ba) are considered as the onset from simple metal to transition metal due to the influence of d electron.[44] Also owing to the effect of d electron, the anomalous phonon features occur in the alkaline-earth metals,[45–47] in particular for Ba where the longitudinal acoustic branch along the $[\xi\ 0\ 0]$ direction is lower than the transverse acoustic branch.[45]

Table III gives the predicted lattice parameters and bulk moduli of Ca, Sr, and Ba at 0 K and 298 K (with both the phonon and electronic contributions), which are in good agreements with the experimental data,[46–49] especially the calculated ones at 298 K, implying the phonon properties will be predicted precisely as demonstrated in the following section. With increasing mass from fcc-Ca, fcc-Sr, to bcc-Ba, their bulk moduli decrease, indicating the weakening of metal bonds. Table III also shows the predicted second-moment Debye temperatures from the phonon DOS's of Ca, Sr, and Ba, which are in prefect agreements with the experiments.[50,51] The change of Debye temperatures from Ca, Sr, to Ba is consistent with the variation of their bulk moduli, confirming the weakening of metal bonds from Ca, Sr, to Ba.

The total electronic DOS's for fcc-Ca, fcc-Sr, and bcc-Ba are illustrated in Fig. 1. It shows that the DOS's of Ca and Sr are quite similar, whereas Ba is a little different from them. Below the Fermi level, their electronic structures are simple and almost free-electron-like. Around the Fermi level, the presence of dip through the sp-d hybridization[44] stabilizes their crystal structures. Above the Fermi level, their electronic structures are somehow complicated by the presence of an empty d band just above the Fermi level.[44,45,47] A transition metal character is present arising from the hybridization with the d band, especially for Ba. The occurrence of bcc structure of Ba in contrast to fcc in Ca and Sr suggests the onset of transition-metal behavior. In addition, Moriarty[44] indicated that the distance of empty d band with respect to

TABLE III. Calculated properties of Ca, Sr, and Ba at 0 K (without phonon contribution) and 298 K (with both phonon and electronic contributions) together with the experimental data: lattice parameter a_0 (Å), bulk modulus B_0 (GPa), and the Debye temperature Θ_D (K).

Material		a_0 (Å)	B_0 (GPa)	Θ_D (K)
fcc-Ca	0 K	5.516	17.32	215[a]
	298 K	5.553	16.00	
	Experiment	5.588[b]	18.3[c]	210[e]
			16.9[d]	229[f]
fcc-Sr	0 K	5.996	11.83	134[a]
	298 K	6.049	10.66	
	Experiment	6.08[b]	14±8[g]	133[e]
				147[f]
bcc-Ba	0 K	4.999	8.99	99[a]
	298 K	5.033	8.40	
	Experiment	5.013[b]	9.4[c]	97[e]
			7±3[g]	110.5[f]

[a]Estimated from the second moment Debye cutoff frequency obtained by phonon DOS.
[b]Reference 48.
[c]Reference 49.
[d]Reference 46.
[e]Reference 50.
[f]Reference 51.
[g]Reference 47.

the Fermi level decreases with increasing of mass among Ca, Sr, and Ba. Further investigation of electronic structure (not shown) indicates that the nonmetal character appears (i.e., the DOS at Fermi level is zero) when the pressure is above about 4 GPa for Ca and 0.5 for Sr. Those phenomena have also been observed experimentally by electronic resistance measurements.[52]

Figure 2 shows the phonon dispersion relations for fcc-Ca, fcc-Sr, and bcc-Ba at their theoretic equilibrium volumes at 0 K. In general, a good agreement is shown between the calculations and the measurements by inelastic neutron scattering.[45,47,53] First of all, the highest frequency decreases from Ca, Sr, to Ba due to the influence of mass. For both Ca and Sr with fcc structures, their dispersion curves are similar to each other. In addition, both of them show that the frequencies of the transverse $T1$ $[\xi\ \xi\ 0]$ (Γ to X, see Fig. 2) branch for ξ at around 0.6 are slightly above the velocity-of-sound line determined from the low frequency measurements.[46,47,53] The present calculations using supercell method also indicate the slightly positive dispersion of the $T1$ branch as shown in Fig. 2. For bcc Ba, the calculated dispersion curves are in good overall agreement with the measurement by coherent inelastic neutron scattering performed on a large single crystal.[45] In the $[\xi\ 0\ 0]$ direction (Γ to H), the calculated longitudinal (L) branch is near to the transverse (T) branches (twofold degenerated) with L laying lower position than T. The predicted anomalous dispersions exhibited by the $[\xi\ 0\ 0]$ branches are in good agreement with

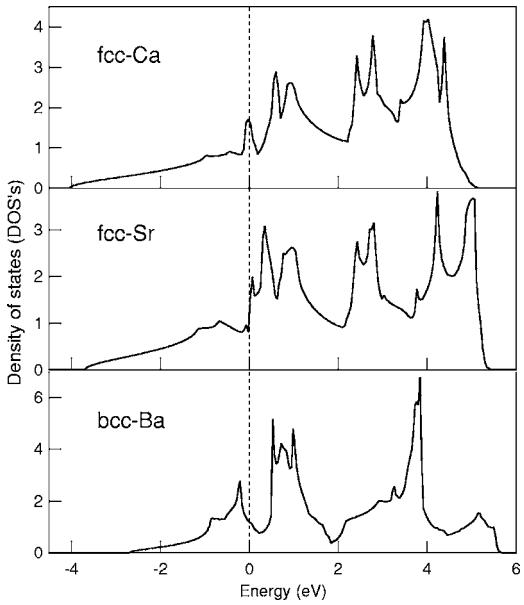

FIG. 1. Total electronic density of states (DOS's) for fcc-Ca, fcc-Sr, and bcc-Ba; the vertical dotted line shows the Fermi level.

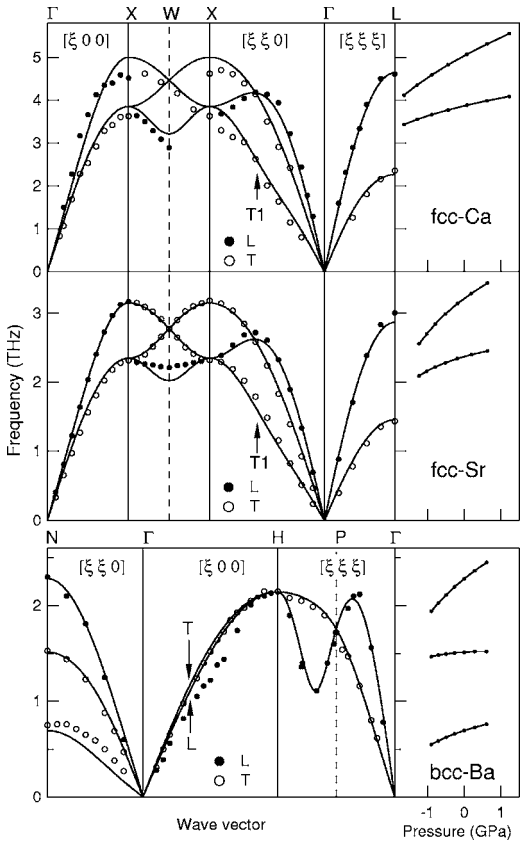

FIG. 2. Calculated phonon dispersion curves for fcc-Ca, fcc-Sr, and bcc-Ba pertaining to the equilibrium volumes at 0 K, and the corresponding data (symbols) measured by inelastic neutron scattering (Refs. 45, 47, and 53). $T1$ indicates the slightly positive dispersion of the transverse branches of fcc-Ca and fcc-Sr. The pressure-dependent frequencies are also shown for the X point (fcc phase) and the N point (bcc phase). The labels T and L indicate the transverse and longitudinal acoustic branches, respectively.

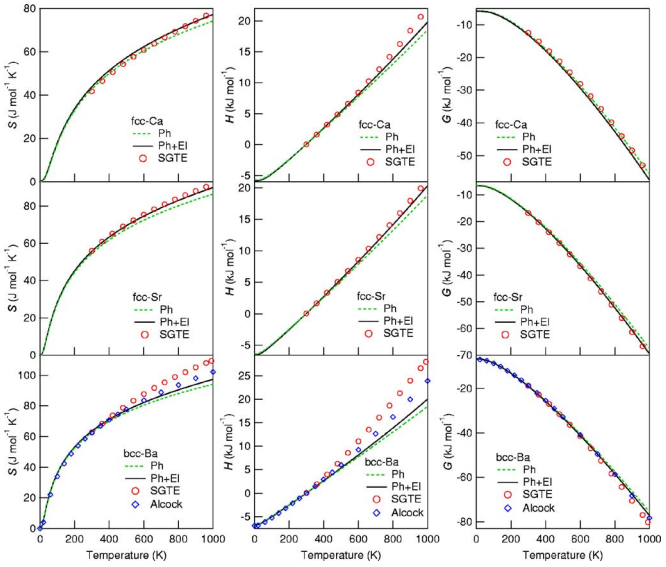

FIG. 3. (Color online) Thermodynamic properties: entropy (S), enthalpy (H), and Gibbs energy (G) for fcc-Ca, fcc-Sr, and bcc-Ba. The lines are the calculated results with ($Ph+El$) and without (Ph) the electronic contributions. The cycles are taken from the SGTE database (Ref. 55). The diamond symbols are recommended data by Alcock *et al.* (Ref. 56).

the measurements. All the anomalous dispersions in Ca, Sr, and Ba can trace their influence by the presence of an empty d band just above the Fermi level.[44,45,47] Both the electronic and phonon features as shown in Figs. 1 and 2 indicate that the divalent alkaline-earth metals (e.g., Ca, Sr, and Ba) are in the middle of simple metal and transition metal. With the variation of external pressure, the phonon frequencies at special points, i.e., the X point of Ca and Sr, and the N point of Ba, are also shown in Fig. 2. For these alkaline-earth metals, the near-linear increasing of phonon frequency with increasing of pressure is predicted. Additionally the highest frequency mode has a larger positive slope than those of others.

Starting from both the electronic and phonon DOS's at several (seven in the present work) different volumes, the free energies (F) of Ca, Sr, and Ba can be predicted based on the quasiharmonic approximation, i.e., Eq. (8). Accordingly, the entropy (S) and internal energy (E) are estimated according to Eqs. (9) and (10), respectively,

$$S = -T\left(\frac{\partial F}{\partial T}\right)_V, \tag{9}$$

$$E = F - T\left(\frac{\partial F}{\partial T}\right)_V, \tag{10}$$

where T and V are temperature and volume, respectively. Neglecting the influence of pressure (P) on solid phase (i.e., the PV term), the internal and free energies are equal to the enthalpy (H) and Gibbs (G) energy, respectively. Figure 3 shows the predicted S, H, and G, where the reference states for H and G are the commonly used setting in the computer coupling of phase diagrams and thermochemistry (CALPHAD) community,[54] i.e., the H at 298 K and 1 bar.

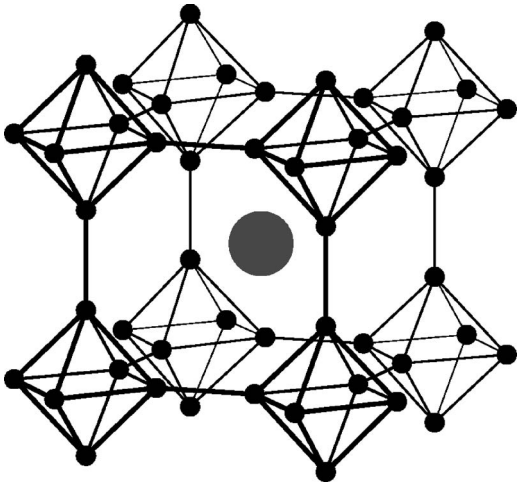

FIG. 4. Crystal structure for the alkaline-earth metal hexaborides MB_6 (M=Ca, Sr, Ba). The large solid cycle is M atom; the small solid cycles are B atoms.

The widely accepted Scientific Group Thermodata Europe (SGTE) data,[55] evaluated from the experimental data, are also given in Fig. 3 for comparison. As expected, Fig. 3 shows that the calculated S, H, and G of Ca, Sr, and Ba have obvious differences with and without the electronic contributions. With the electronic contributions, the calculated values of S and H increase, but the calculated values of G decrease. There are perfect agreements between measurements (SGTE data) and calculations (including both the electronic and phonon contributions) for Ca and especially for Sr. For bcc Ba, the calculated G agrees with the SGTE data, but for S and H there are big differences between calculations and the SGTE data. Note that because the alkaline-earth metals, in particular Ba, are highly reactive metals, it is inevitable that oxygen and hydrogen can easily contaminate samples and generate significant thermal effects during measurements at elevated temperatures, making all available data above room temperature unreliable. The uncertainty in the reported thermodynamic values usually exceeds 15% for Ba.[56] Based on this consideration, the recommended data of bcc-Ba by Alcock *et al.*[56] are also shown in Fig. 3, which are close to the present predictions. By considering the accurately predicted phonon dispersion curves for Ca, Sr, and Ba (see Fig. 2) and the accurately predicted thermodynamic data for Ca and Sr, it is suggested that the present calculated thermodynamic data can be considered as tentative for the further measurements of thermodynamic data of Ba.

C. CaB_6, SrB_6, and BaB_6

The divalent alkaline-earth hexaborides MB_6 (M=Ca, Sr, and Ba) have a bcc-like structure with space group of $Pm\bar{3}m$, in which metal ions M locate at the Wyckoff position $1a$ (0, 0, 0) and octahedral B_6 at the Wyckoff position $6f$ (x, 1/2, 1/2), as shown in Fig. 4. The structure information is determined by the lattice parameter a and the positional parameter x (usually $x<0.207$). When $x=0.207$, the intraoctahedral and interoctahedral B-B distances become indistinguishable; see

TABLE IV. Calculated properties of hexaborides MB_6 (M=Ca,Sr,Ba), at 0 K (without phonon contribution) and 298 K (with both phonon and electronic contributions) together with the experimental data: lattice parameter a_0 (Å), positional parameter x in Wyckoff position 6f (x, 1/2, 1/2) of B atoms, bulk modulus B_0 (GPa), Debye temperature Θ_D (K), and enthalpy of formation ΔH (kJ/mol).

Material		a_0 (Å)	x	B_0 (GPa)	Θ_D (K)	ΔH (kJ/mol)
CaB_6	0 K	4.148	0.2018	149.04	1289[a]	−40.774
	298 K	4.168		138.59		−40.742
	Experiment	4.1514[b]	0.2019[b]	151[c]	783[e]	−17.078[f]
				149[d]		
SrB_6	0 K	4.198	0.2031	147.43	1259[a]	−44.794
	298 K	4.217		141.08		−44.920
	Experiment	4.1953[b]	0.2031[b]		736[g]	−30.096[f]
BaB_6	0 K	4.2787	0.2054	144.33	1202[a]	−40.543
	298 K	4.2967		138.58		−40.991
	Experiment	4.2618[b]	0.2047[b]			−47.533[f]

[a]Estimated from the second-moment Debye cutoff frequency obtained by phonon DOS.
[b]Reference 15.
[c]Calculated value by LDA (Ref. 9).
[d]Calculated value by sX-LDA (Ref. 9).
[e]Estimated value through low-temperature specific heat below 11 K (Ref. 58).
[f]Reference 12.
[g]Estimated value through low-temperature specific heat below 8.9 K (Ref. 59).

Fig. 4. It has been demonstrated that the band gap at the X point of MB_6 is sensitive and proportional to the values of a and x.[9,57] The present calculated structure parameters are in excellent agreement with experiments[9,12,15,58,59] as shown Table IV. For CaB_6, SrB_6, and BaB_6, the values of a and x increase with increasing of mass. The predicted x value less than 0.207 indicates that the interoctahedral B-B distance is less than the intraoctahedral B-B distance. Table IV also shows that the predicted bulk moduli of CaB_6, SrB_6, and BaB_6 are close to each other. The present bulk modulus of CaB_6 agree with the calculated ones by LDA and sX-LDA.[9]

The total electronic DOS's around the Fermi level of CaB_6, SrB_6, and BaB_6 are shown in Fig. 5. In general, the basic features of these electronic structures are similar. Furthermore, the DOS of CaB_6 is rather closer to that of SrB_6, while the DOS of BaB_6 is somewhat complex because the electronic structure of Ba is closer to transition metal than those of Ca and Sr. Although the presently predicted electronic structure is in gross agreement with the predictions by WDA,[8] xS-LDA,[9] and GW approximation,[4] the DOS's around the Fermi level clearly indicates a semimetal characteristic rather than an experimental semiconductor,[7,10] due to the fact that LDA and GGA approximations are usually underestimate the band gap of semiconductor. However, the capacity of GGA to predict accurate structure properties (see Table IV) implies that the phonon calculations also would be accurate.

Figure 6 shows the calculated phonon dispersion relations for CaB_6, SrB_6, and BaB_6. The general features of them are identical except that the frequencies decrease from CaB_6, SrB_6, to BaB_6 due to the influence of mass, indicating the similar properties of divalent alkaline-earth hexaborides. At the Γ point, a group theory analysis[60] leads to the following vibrational modes for Wyckoff positions 1a and 6f of space group $Pm\bar{3}m$,

$$\Gamma(1a, Pm\bar{3}m) = T_{1u}(\mathrm{IR}), \tag{11a}$$

$$\Gamma(6f, Pm\bar{3}m) = A_{1g}(\mathrm{R}) + E_g(\mathrm{R}) + T_{2u} + T_{2g}(\mathrm{R}) + 2T_{1u}(\mathrm{IR}) + T_{1g}, \tag{11b}$$

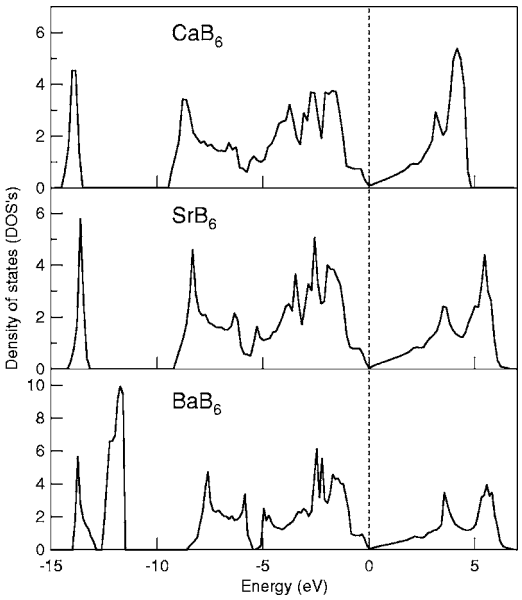

FIG. 5. Total electronic density of states (DOS's) for CaB_6, SrB_6, and BaB_6; the vertical dotted line shows the Fermi level.

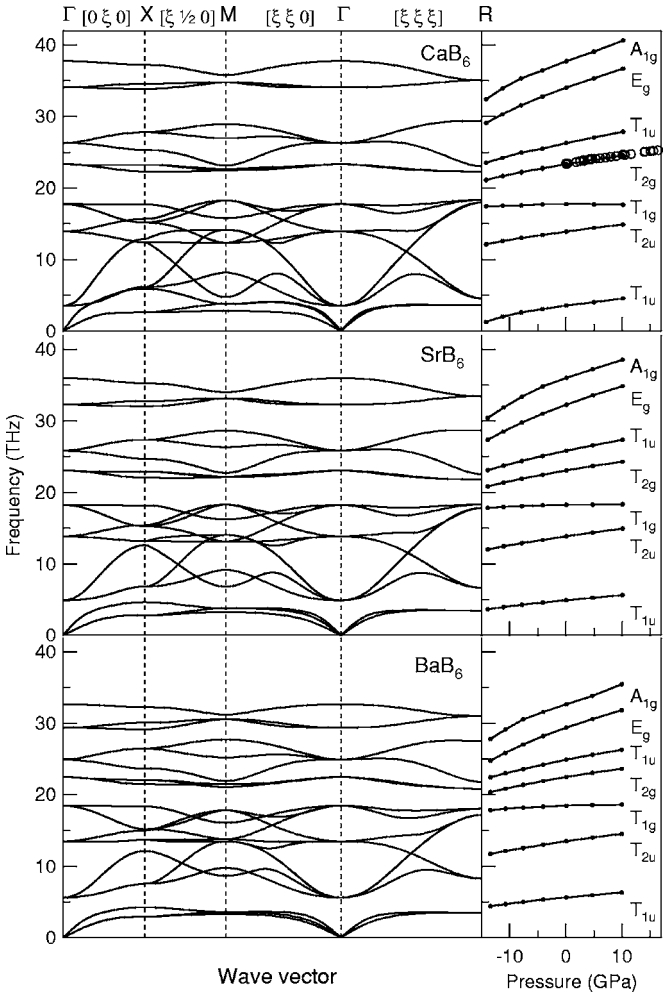

FIG. 6. Calculated phonon dispersion curves of CaB_6, SrB_6, and BaB_6 pertaining to the equilibrium volumes at 0 K. The pressure-dependent frequencies at the Γ point are also shown, together with the measured T_{2g} modes (Ref. 66) (open circles) for CaB_6. Note that the LO/TO splitting is not shown for the infrared active T_{1u} modes (see Sec. IV C).

where R and IR indicate the Raman and infrared active modes, respectively. The sketches of these phonon modes in Eq. (11) can be found in Refs. 61 and 62.

At the Γ point, the present calculated optical phonon modes of CaB_6, SrB_6, and BaB_6 pertaining to the equilibrium volumes at 0 K are given in Table V, which are in excellent agreements with the available Raman and infrared measurements.[2,7,63–65] To our knowledge, there are no available measurements for BaB_6; however, it is believed that the present calculations are rather accurate according to the following two facts: (i) the phonon modes should be similar among the divalent alkaline-earth hexaboride, and (ii) a decreasing trend of phonon frequency is present with increasing the mass of metal in the divalent alkaline-earth hexaboride (or the lattice parameter).[61,64] As shown in Table V, the sX-LDA calculated T_{2g} mode of CaB_6 (the breathing mode is indicated in Ref. 9; however, it should be the T_{2g} mode according to the reported value) is about 3 THz lower that the experimental observations, and it can be understood that the force constants are not predicted correctly, although sX-LDA predicted the correct band gap of CaB_6. The pressure-dependent optical modes at the Γ point are also illustrated in Fig. 6. A linear increasing trend with respect to external pressure is shown for these modes except for the T_{1g} mode with a pressure-independent characteristic. The predicted pressure-dependent T_{2g} mode for CaB_6 agrees well with the Raman measurements.[66]

The present calculations (see Fig. 5) show that the divalent hexaborides CaB_6, SrB_6, and BaB_6 are semimetals, even having zero electronic densities at the Fermi levels. In principle, the long range of the Coulomb interactions in these ionic compounds should cause the frequencies of longitudinal optical (LO) modes above those of transversal optical (TO) modes.[67] The LO/TO splitting occurs at the Γ point of the Brillouin zone, and only for infrared active modes, e.g., the T_{1u} modes for the hexaborides. The supercell method used above cannot be employed to estimate the LO/TO splitting directly, because only finite wave vector $\xi \neq 0$ calcula-

TABLE V. Calculated and measured optical frequencies (in THz) at the Γ point for the hexaborides MB_6 (M=Ca, Sr, Ba), where R represents Raman mode, IR infrared mode.

Material		A_{1g} (R)	E_g (R)	T_{1u} (IR)	T_{2g} (R)	T_{1g}	T_{2u}	T_{1u} (IR)
CaB_6	This work	37.74	34.06	26.29	23.33	17.73	13.90	3.56
	Ref. 7							4.48
	Ref. 9				20.4[a], 23.5[b]			
	Ref. 63	38.5[c]	34.5[c]		23.4[c]			
	Ref. 64	38.07	33.73		23.23			
	Ref. 65	37.38	33.64		22.60			
	Ref. 2	37.77	33.61		22.99			
SrB_6	This work	36.00	32.28	25.83	23.09	18.26	13.86	4.93
	Ref. 64	36.72	33.13		23.08			
BaB_6	This work	32.66	29.39	24.90	22.49	18.45	13.50	5.63

[a]Calculated by sX-LDA.
[b]Calculated by LDA.
[c]Measured at 13 K.

tions are possible. Therefore, the elongated supercells are needed to recover the wave vector $\xi \rightarrow 0$ limit of the LO optical branches.[67] In the present work, the elongated supercell $1\times1\times10$ and the PHONON code[68] are employed to probe the appearances of LO/TO splitting for the hexaborides. It is found that the LO/TO splitting appears obviously for the low frequency T_{1u} modes (with frequencies around 5 THz, see Table V). The predicted frequencies of the LO modes are 11.8, 11.6, and 11.2 THz for CaB_6, SrB_6, and BaB_6, respectively. However, for the high frequency T_{1u} modes (with frequencies around 25 THz, see Table V), no obvious LO/TO splitting appears. It should be mentioned that the LO modes contribute very little to the phonon DOS's, since they differ from TO modes only in a small volume of the reciprocal lattice in the vicinity of the Γ point. Therefore, the influences of LO/TO splitting on the predicted properties are not taken into account in the present work.

On the basis of the second-moment Debye cutoff frequency estimated from the phonon DOS's, the Debye temperatures of CaB_6, SrB_6, and BaB_6 are calculated and shown in Table IV. The predicted Debye temperatures are much higher than the measured values[58,59] obtained through the data of low temperature (<11 K) specific heat. It is argued that the measured Debye temperatures from the heat capacity at low temperatures are inconsistent with the high melting points and the low coefficients of thermal expansion characteristic of the hexaborides.[1] As indicated by Mandrus *et al.*[69] for LaB_6, the Debye temperature obtained from the heat capacity in low temperature are around 250 K, mainly reflecting the contribution of the La local mode. However, the obtained Debye temperature for LaB_6 is 1160 K from the room temperature crystallography data.[69] Due to the lattice properties of B-rich compounds depend mainly on the B-B bonding, and the melting point of MB_6 is comparable with those of $B_{12}C_3$, β-B, and YB_{66},[70] with the Debye temperature of β-B reported to be 1300 K (see Table II), the present predicted Debye temperatures of CaB_6, SrB_6, and BaB_6 are more reasonable.

In terms of the quasiharmonic approximation, Fig. 7 shows the predicted thermodynamic properties for CaB_6, SrB_6, and BaB_6, including entropy (S), enthalpy (H), and Gibbs (G) energy. It is shown that the electronic contributions are negligible due to the lower electronic DOS's near the Fermi level (see Fig. 5). In fact, the electronic contributions can be neglected safely owing to the semiconductor natures of the divalent alkaline-earth hexaborides, just as the previous treatments for α- and β-B. Using results shown in Ref. 32 and Figs. 4 and 7, the predicted enthalpies of formation for CaB_6, SrB_6, and BaB_6 are shown in Table IV together with the experimental data.[12] Large differences between measurements and calculations are noticed for CaB_6 and SrB_6. This may be because the measurements for CaB_6 and SrB_6 were conducted at very high temperatures. In contract to the big differences of the measured enthalpies of formation among CaB_6, SrB_6, and BaB_6, this work predicts similar enthalpies of formation, which agree with the facts that they have the similar melting temperatures,[1,2] standard entropies,[12] bulk moduli, and Debye temperatures (see Table IV).

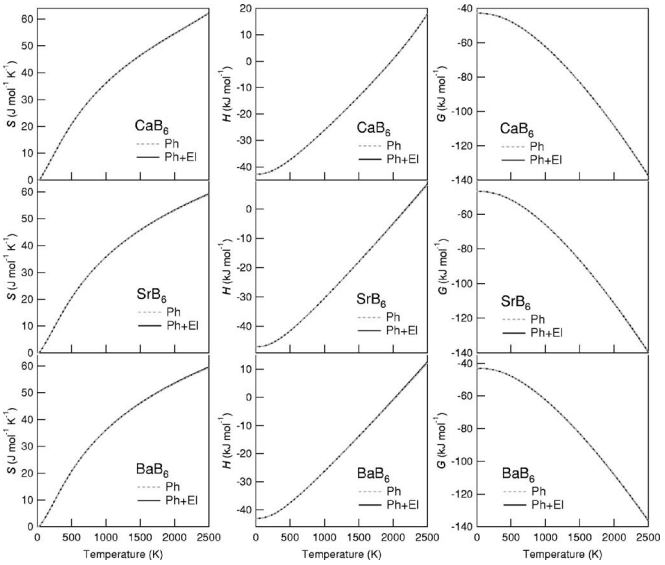

FIG. 7. Thermodynamic properties: entropy (S), enthalpy (H), and Gibbs energy (G) for CaB_6, SrB_6, and BaB_6. The lines are the calculated results with ($Ph+El$) and without (Ph) the electronic contributions.

V. CONCLUSIONS

In terms of first-principles quasiharmonic phonon calculations, the phonon and thermodynamic properties have been investigated for the divalent alkaline-earth hexaborides, MB_6 (M=Ca, Sr, and Ba), and the reference elements B, Ca, Sr, and Ba. The calculated phonon dispersion relations using the supercell approach are in good agreements with those obtained by the inelastic neutron scattering, Raman scattering, and infrared absorption. The experimentally revealed anomalous behaviors of phonon dispersions in the alkaline-earth metals are correctly predicted; i.e., for both fcc-Ca and fcc-Sr, the frequency of the lower transverse $[\xi\ \xi\ 0]$ branch exhibits slightly positive dispersion, and for bcc-Ba the frequency of longitudinal branch along the $[\xi\ 0\ 0]$ direction is lower than that of the transverse branch. These anomalous phenomena of alkaline-earth elements can be traced back to the effects of d electrons. The predicted phonon dispersion relations among CaB_6, SrB_6, and BaB_6 show similar features except the frequencies decrease from CaB_6, SrB_6, to BaB_6 due to the influence of mass. It is also found that the low frequency T_{1u} modes of CaB_6, SrB_6, and BaB_6 have large LO/TO splitting (greater than 5 THz). To that end, the finite temperature thermodynamic properties (entropy, enthalpy, and Gibbs energy) of hexaborides CaB_6, SrB_6, BaB_6, and elements B, Ca, Sr, and Ba are calculated; herein, both the phonon and electronic contributions are considered. This work indicates that the difference of the enthalpies of formation of CaB_6, SrB_6, and BaB_6 is small, which agrees with the facts that they possess similar phonon dispersion relations, melting temperatures, bulk moduli, and Debye temperatures. The thermodynamic descriptions obtained here can be used for better fabrication of these alkaline-earth hexaborides CaB_6, SrB_6, and BaB_6, which continue to garner interest in the scientific community.

ACKNOWLEDGMENTS

This work is funded by the National Science Foundation (NSF) through Grant No. DMR-0510180. First-principles calculations are carried out on the LION clusters at the Pennsylvania State University supported in part by the NSF Grants No. DMR-9983532, No. DMR-0122638, and No. DMR-0205232) and in part by the Materials Simulation Center and the Graduate Education and Research Services at the Pennsylvania State University.

*Electronic address: sus26@psu.edu

[1] R. M. Adams, *Boron, Metallo-Boron Compounds, and Boranes* (Interscience Publishers, New York, 1964).
[2] T. T. Xu, J. G. Zheng, A. W. Nicholls, S. Stankovich, R. D. Piner, and R. S. Ruoff, Nano Lett. **4**, 2051 (2004).
[3] D. P. Young, D. Hall, M. E. Torelli, Z. Fisk, J. L. Sarrao, J. D. Thompson, H. R. Ott, S. B. Oseroff, R. G. Goodrich, and R. Zysler, Nature **397**, 412 (1999).
[4] H. J. Tromp, P. van Gelderen, P. J. Kelly, G. Brocks, and P. A. Bobbert, Phys. Rev. Lett. **87**, 016401 (2001).
[5] J. D. Denlinger, J. A. Clack, J. W. Allen, G. H. Gweon, D. M. Poirier, C. G. Olson, J. L. Sarrao, A. D. Bianchi, and Z. Fisk, Phys. Rev. Lett. **89**, 157601 (2002).
[6] S. Souma, H. Komatsu, T. Takahashi, R. Kaji, T. Sasaki, Y. Yokoo, and J. Akimitsu, Phys. Rev. Lett. **90**, 027202 (2003).
[7] B. K. Cho, J. S. Rhyee, B. H. Oh, M. H. Jung, H. C. Kim, Y. K. Yoon, J. H. Kim, and T. Ekino, Phys. Rev. B **69**, 113202 (2004).
[8] Z. G. Wu, D. J. Singh, and R. E. Cohen, Phys. Rev. B **69**, 193105 (2004).
[9] B. Lee and L. W. Wang, Appl. Phys. Lett. **87**, 262509 (2005).
[10] S. Souma, T. Takahashi, H. Komatsu, T. Sato, H. Matsui, N. Kimura, H. Aoki, S. Kunii, and J. Akimitsu, Phys. Rev. B **70**, 073104 (2004).
[11] M. C. Bennett, J. van Lierop, E. M. Berkeley, J. F. Mansfield, C. Henderson, M. C. Aronson, D. P. Young, A. Bianchi, Z. Fisk, F. Balakirev, and A. Lacerda, Phys. Rev. B **69**, 132407 (2004).
[12] G. V. Samsonov and I. M. Vinitskii, *Handbook of Refractory Compounds* (Plenum Press, New York, 1980).
[13] H. Kino, F. Aryasetiawan, K. Terakura, and T. Miyake, Phys. Rev. B **66**, 121103(R) (2002); H. Kino, F. Aryasetiawan, M. van Schilfgaarde, T. Kotani, T. Miyake, and K. Terakura, J. Phys. Chem. Solids **63**, 1595 (2002).
[14] A. Schindlmayr, T. J. Pollehn, and R. W. Godby, Phys. Rev. B **58**, 12684 (1998).
[15] C. H. Chen, T. Aizawa, N. Iyi, A. Sato, and S. Otani, J. Alloys Compd. **366**, L6 (2004).
[16] S. P. Gao, J. Jiang, M. Cao, J. Zhu, and J. Yuan, Phys. Rev. B **69**, 214419 (2004).
[17] S. Baroni, S. de Gironcoli, A. Dal Corso, and P. Giannozzi, Rev. Mod. Phys. **73**, 515 (2001); A. van de Walle and G. Ceder, *ibid.* **74**, 11 (2002).
[18] Y. Wang, Z. K. Liu, and L. Q. Chen, Acta Mater. **52**, 2665 (2004).
[19] E. Kaxiras, *Atomic and Electronic Structure of Solids* (Cambridge University Press, New York, 2003).
[20] K. Parlinski, Z-. Q. Li, and Y. Kawazoe, Phys. Rev. Lett. **78**, 4063 (1997).
[21] R. Arroyave, D. Shin, and Z. K. Liu, Acta Mater. **53**, 1809 (2005).
[22] A. L. Goodman, J. Phys. G **16**, 1557 (1990).
[23] S. Shang and A. J. Böttger, Acta Mater. **53**, 255 (2005).
[24] G. Kresse and D. Joubert, Phys. Rev. B **59**, 1758 (1999); P. E. Blöchl, *ibid.* **50**, 17953 (1994).
[25] G. Kresse and J. Furthmüller, Phys. Rev. B **54**, 11169 (1996); Comput. Mater. Sci. **6**, 15 (1996).
[26] J. P. Perdew and Y. Wang, Phys. Rev. B **45**, 13244 (1992).
[27] A. van de Walle, M. Asta, and G. Ceder, CALPHAD: Comput. Coupling Phase Diagrams Thermochem. **26**, 539 (2002).
[28] H. J. Monkhorst and J. D. Pack, Phys. Rev. B **13**, 5188 (1976).
[29] P. E. Blöchl, O. Jepsen, and O. K. Andersen, Phys. Rev. B **49**, 16223 (1994).
[30] M. I. Eremets, V. W. Struzhkin, H. K. Mao, and R. J. Hemley, Science **293**, 272 (2001).
[31] R. Naslain, in *Boron and Refractory Borides*, edited by V. I. Matkovich (Springer-Verlag, New York, 1977), p. 139.
[32] S. Shang, Y. Wang, R. Arroyave, and Z.-K. Liu (unpublished).
[33] G. H. Wolf and R. Jeanloz, Phys. Rev. B **32**, 7798 (1985).
[34] M. Fujimori, T. Nakata, T. Nakayama, E. Nishibori, K. Kimura, M. Takata, and M. Sakata, Phys. Rev. Lett. **82**, 4452 (1999).
[35] R. J. Nelmes, J. S. Loveday, D. R. Allan, J. M. Besson, G. Hamel, P. Grima, and S. Hull, Phys. Rev. B **47**, 7668 (1993).
[36] D. N. Sanz, P. Loubeyre, and M. Mezouar, Phys. Rev. Lett. **89**, 245501 (2002).
[37] G. A. Slack, D. W. Oliver, and F. H. Horn, Phys. Rev. B **4**, 1714 (1971).
[38] B. Callmer, Acta Crystallogr., Sect. B: Struct. Crystallogr. Cryst. Chem. **B33**, 1951 (1977).
[39] T. Lundstrom, B. Lonnberg, and J. Bauer, J. Alloys Compd. **267**, 54 (1998).
[40] J. L. Hoard, D. B. Sullenger, C. H. L. Kennard, and R. E. Hughes, J. Solid State Chem. **1**, 268 (1970); G. A. Slack, C. I. Hejna, M. F. Garbauskas, and J. S. Kasper, *ibid.* **76**, 52 (1988).
[41] Y. Chen, K. M. Ho, B. N. Harmon, and C. Stassis, Phys. Rev. B **33**, 3684 (1986); J. E. Hearn, R. L. Johnston, S. Leoni, and J. N. Murrell, J. Chem. Soc., Faraday Trans. **92**, 425 (1996).
[42] E. Y. Tonkov and E. G. Ponyatovsky, *Phase Transformations of Elements under High Pressure* (CRC Press, Boca Raton, FL, 2005).
[43] G. M. Wang, D. A. Papaconstantopoulos, and E. Blaisten-Barojas, J. Phys. Chem. Solids **64**, 185 (2003).
[44] J. A. Moriarty, Phys. Rev. B **34**, 6738 (1986).
[45] J. Mizuki, Y. Chen, K. M. Ho, and C. Stassis, Phys. Rev. B **32**, 666 (1985).
[46] M. Heiroth, U. Buchenau, H. R. Schober, and J. Evers, Phys. Rev. B **34**, 6681 (1986).
[47] U. Buchenau, M. Heiroth, H. R. Schober, J. Evers, and G. Oehlinger, Phys. Rev. B **30**, 3502 (1984).
[48] P. Villars and L. D. Calvert, *Pearson's Handbook of Crystallographic Data for Intermetallic Phases*, 2nd ed. (ASTM International, Newbury, OH, 1991).

[49] S. N. Vaidya and G. C. Kennedy, J. Phys. Chem. Solids **31**, 2329 (1970).
[50] J. G. Cook and M. P. Vanderme, J. Phys. F: Met. Phys. **3**, 130 (1973).
[51] G. K. White, J. Phys. F: Met. Phys. **2**, 865 (1972).
[52] R. A. Stager and H. G. Drickamer, Phys. Rev. **131**, 2524 (1963).
[53] C. Stassis, J. Zaretsky, D. K. Misemer, H. L. Skriver, B. N. Harmon, and R. M. Nicklow, Phys. Rev. B **27**, 3303 (1983).
[54] N. Saunders and A. P. Miodownik, *CALPHAD (Calculation of Phase Diagrams): A Comprehensive Guide* (Pergamon, New York, 1998).
[55] A. T. Dinsdale, CALPHAD: Comput. Coupling Phase Diagrams Thermochem. **15**, 317 (1991).
[56] C. B. Alcock, M. W. Chase, and V. Itkin, J. Phys. Chem. Ref. Data **22**, 1 (1993).
[57] K. Schmitt, C. Stuckl, H. Ripplinger, and B. Albert, Solid State Sci. **3**, 321 (2001).
[58] P. Vonlanthen, E. Felder, L. Degiorgi, H. R. Ott, D. P. Young, A. D. Bianchi, and Z. Fisk, Phys. Rev. B **62**, 10076 (2000).
[59] H. R. Ott, M. Chernikov, E. Felder, L. Degiorgi, E. G. Moshopoulou, J. L. Sarrao, and Z. Fisk, Z. Phys. B: Condens. Matter **102**, 337 (1997).
[60] M. I. Aroyo, A. Kirov, C. Capillas, J. M. Perez-Mato, and H. Wondratschek, Acta Crystallogr., Sect. A: Found. Crystallogr. **A62**, 115 (2006).
[61] N. Ogita, S. Nagai, N. Okamoto, M. Udagawa, F. Iga, M. Sera, J. Akimitsu, and S. Kunii, Phys. Rev. B **68**, 224305 (2003).
[62] G. Schell, H. Winter, H. Rietschel, and F. Gompf, Phys. Rev. B **25**, 1589 (1982).
[63] N. Ogita, S. Nagai, N. Okamoto, F. Iga, S. Kunii, T. Akamtsu, J. Akimitsu, and M. Udagawa, J. Solid State Chem. **177**, 461 (2004).
[64] Z. Yahia, S. Turrell, J. P. Mercurio, and G. Turrell, J. Raman Spectrosc. **24**, 207 (1993).
[65] L. Shi, Y. L. Gu, L. Y. Chen, Z. C. Yang, J. H. Ma, and Y. T. Qian, Chem. Lett. **32**, 958 (2003).
[66] N. Ogita, S. Nagai, M. Udagawa, F. Iga, M. Sera, T. Oguchi, T. Akimitsu, and S. Kunii, Physica B **359**, 941 (2005).
[67] K. Parlinski, J. Alloys Compd. **328**, 97 (2001); K. Parlinski, J. Łażewski, and Y. Kawazoe, J. Phys. Chem. Solids **61**, 87 (2000); J. Łażewski, K. Parlinski, W. Szuszkiewicz, and B. Hennion, Phys. Rev. B **67**, 094305 (2003).
[68] K. Parlinski, PHONON 4.22 (2003). The PHONON code is only used to check the appearance of LO/TO splitting in the hexaborides due to the convenience of usage, wherein the needed force constants are calculated by the VASP code (Ref. 25) with the $10\times10\times1$ Monkhorst-Pack (Ref. 28) k mesh, the other settings are the same as those shown in Table I.
[69] D. Mandrus, B. C. Sales, and R. Jin, Phys. Rev. B **64**, 012302 (2001).
[70] T. Tanaka, J. Phys. C **7**, L177 (1974).